MicroRNA-145 promotes the epithelial-mesenchymal transition in peritoneal dialysis-associated fibrosis by suppressing fibroblast growth factor 10

Received for publication, January 6, 2019, and in revised form, August 14, 2019 Published, Papers in Press, August 20, 2019, DOI 10.1074/jbc.RA119.007404

Jiayu Wu[‡1], Qianyin Huang[‡1], Peilin Li[‡1], Yuxian Wang[§], Chenghao Zheng[¶], Xianghong Lei[‡], Shuting Li[‡], Wangqiu Gong[‡], Bohui Yin[‡], Congwei Luo[‡], Jing Xiao[‡], Weidong Zhou[‡], Zhaozhong Xu[‖], Yihua Chen[‡2], Fenfen Peng[‡3], and Haibo Long[‡4]

*From the Departments of [‡]Nephrology, [§]Gerontology, and [‖]Emergency, Zhujiang Hospital, Southern Medical University, Guangzhou 510280, China and the [¶]*Second Clinical Medical School, Southern Medical University, Guangzhou 510280, China

Edited by Xiao-Fan Wang

Peritoneal fibrosis is a common complication of long-term peritoneal dialysis (PD) and the principal cause of ultrafiltration failure during PD. The initial and reversible step in PD-associated peritoneal fibrosis is the epithelial-mesenchymal transition (EMT). Although the mechanisms in the EMT have been the focus of many studies, only limited information is currently available concerning microRNA (miRNA) regulation in peritoneal fibrosis. In this study, we aimed to characterize the roles of microRNA-145 (miR-145) and fibroblast growth factor 10 (FGF10) in peritoneal fibrosis. After inducing EMT with transforming growth factor-β1 (TGF-β1) *in vitro*, we found that miR-145 is significantly up-regulated, whereas FGF10 is markedly down-regulated, suggesting a close link between miR-145 and FGF10 in peritoneal fibrosis, further confirmed in luciferase reporter experiments. Furthermore, in human peritoneal mesothelial cells (*i.e.* HMrSV5 cells), miR-145 mimics induced EMT, whereas miR-145 inhibition suppressed EMT, and we also observed that miR-145 suppressed FGF10 expression. *In vivo*, we found that the exogenous delivery of an miR-145 expression plasmid both blocked FGF10 and intensified the EMT, whereas miR-145 inhibition promoted the expression of FGF10 and reversed the EMT. In conclusion, miR-145 promotes the EMT during the development of peritoneal fibrosis by suppressing FGF10 activity, suggesting that miR-145 represents a potential therapeutic target for managing peritoneal fibrosis.

It has been demonstrated that long-term peritoneal dialysis (PD)[5] can contribute to morphologic changes in the peritoneum, including the loss of mesothelial cells (MCs), accumulation of extracellular matrix, and formation of fibrosis (1). Currently, PD is recognized as a home-based renal replacement therapy; moreover, the improvements in clinical outcomes and demonstration of the socioeconomic benefits of PD have led several countries to adopt policies that favor the use of this modality as the initial renal replacement therapy (2, 3). Recent studies have reported that MCs play a critical role in the development of peritoneal fibrosis through phenotype transition, which disrupts the tight junction and results in MCs acquiring a migratory and invasive phenotype with the production of extracellular matrix (4–7). MCs are the first barrier to the solution used in PD, as they cover the surface of the peritoneal membrane. Moreover, MCs regulate serosal homeostasis and leukocyte trafficking through repairing after injury. If the normal repair functions break down, they will produce factors that actively affect coagulation, such as profibrotic factors, cytokines, and chemokines (8). At the beginning of peritoneal dialysis, epithelial-mesenchymal transition (EMT) of MCs is a frequent pathological change of the peritoneal membrane, which is also related to the high solute transport status and will ultimately cause ultrafiltration failure (9).

MicroRNAs (miRNAs) are small noncoding RNA molecules that play a complex role in the regulation of post-transcriptional expression by binding to 3′-untranslated regions (3′-UTRs) of mRNA (10). Currently, emerging evidence indicates that the regulation of post-transcriptional expression by miRNAs plays an important role in the pathogenesis of peritoneal

This work was supported by the National Natural Science Foundation of China (NSFC) Grants 81673792, 81600624, 81704134, 81873346, and U1801288; Natural Science Foundation of Guangdong Province, China, Grants 2017A030313708 and 2014A030310065; Science and Technology Planning Project of Guangdong Province, China, Grants 2014A020210011, 2015A020211012, and 2017A020215158; and Science and Technology Planning Project of Guangzhou, China, Grants 201510010137 and 201707010286. The authors declare that they have no conflicts of interest with the contents of this article.

This article contains Figs. S1–S4 and Sequences S1–S4.

[1] These authors contributed equally to this work.

[2] To whom correspondence may be addressed: Dept. of Nephrology, Zhujiang Hospital, Southern Medical University, Guangzhou 510280, China. Tel./Fax: 86-20-6278-2305; E-mail: 13724005373@163.com.

[3] To whom correspondence may be addressed: Dept. of Nephrology, Zhujiang Hospital, Southern Medical University, Guangzhou 510280, China. Tel./Fax: 86-20-6728-2305; E-mail: doctorpff@163.com.

[4] To whom correspondence may be addressed: Dept. of Nephrology, Zhujiang Hospital, Southern Medical University, Guangzhou 510280, China. Tel./Fax: 86-20-6728-2305; E-mail: longhb1966@163.com.

[5] The abbreviations used are: PD, peritoneal dialysis; 3′-UTR, 3′-untranslated region; α-SMA, α-smooth muscle actin; Col1α1, collagen I α1; ctrl inhibitor, control miR-145 inhibitor; ctrl mimics, control miRNA mimics; E-cad, E-cadherin; EMT, epithelial-mesenchymal transition; FGF10, fibroblast growth factor 10; FN1, fibronectin 1; MC, mesothelial cell; miR-145, microRNA-145; miRNA, microRNA; PDF, peritoneal dialysis fluid; si-FGF10, FGF10 siRNA; TGF-β1, transforming growth factor-β1; EMT-TFs, EMT-inducing transcription factors; GAPDH, glyceraldehyde-3-phosphate dehydrogenase; HSC, hepatic stellate cell; qPCR, quantitative PCR.

fibrosis. For example, a recent study demonstrated that miR-15a-5p suppresses the inflammatory and fibrotic activities of peritoneal MCs induced by PD via inhibiting vascular endothelial growth factor A directly (11). Moreover, both miR-199a-5p and miR-214-3p were found to target claudin-2 and E-cadherin (E-cad) mRNAs to promote high glucose–induced peritoneal fibrosis in PD (12). In addition, human umbilical cord mesenchymal stem cells facilitate the up-regulation of miR-153-3p, which is a critical molecule in attenuating methylglyoxal-induced peritoneal fibrosis in rats (13). Specifically, miR-21 was shown to promote the progression of peritoneal fibrosis through activating the TGF-β/Smad signaling pathway in *in vivo* and *in vitro* experiments (14). In fact, miR-129-5p was reported to directly target the 3′-UTR of the Smad-interacting protein 1 (*SIP1*) and SRY-box 4 (*SOX4*) genes and repress their post-transcriptional activities to modulate the EMT and fibrosis in the setting of PD (15). Furthermore, it was shown that miR-30a negatively regulates transforming growth factor-β1 (TGF-β1)-induced EMT and peritoneal fibrosis by targeting Snai1 *in vivo* and vitro, with improvement of peritoneal dysfunction (16). miR-30b directly targeted and inhibited bone morphogenetic protein 7 (BMP7) by binding to its 3′-UTR to regulate methylglyoxal-induced EMT of peritoneal MCs in rats (17).

Among these miRNAs, microRNA-145 (miR-145) is of significant interest to our group because it can be up-regulated by TGF-β in fibrotic disease (18). In addition, microRNA-145 antagonism reverses the TGF-β inhibition of F508del cystic fibrosis transmembrane conductance regulator correction in airway epithelia (19). Furthermore, it was reported that miR-145 was up-regulated in activated rat primary hepatic stellate cells (HSCs) and TGF-β–treated HSCs, which contributed to liver fibrosis (20). However, whether miR-145 regulates peritoneal fibrosis in the development of PD remains unknown.

Fibroblast growth factor 10 (FGF10) has been found in all examined vertebrates, and it is a multifunctional mesenchymal-epithelial signaling growth factor that is essential for multiorgan development and tissue homeostasis in adults (21, 22). FGF10, a member of the family of fibroblast growth factors (FGFs), was generated from a common ancestral gene during the early evolution of vertebrates and retains similar amino acid sequences and biochemical functions (23). It has been shown that FGF10 activates key intracellular signaling pathways in some cell types, contributing to cell proliferation, differentiation, and migration during development and the modulation of organ branching (24). Recent studies have shown that FGF10 reduces bleomycin-induced lung fibrosis, possibly through its AT2-protective effects (25). Furthermore, FGF10/FGFR2 and androgen receptor were reduced in renal fibrosis in adult male rat offspring subjected to prenatal exposure to di-*n*-butyl phthalate, but the concrete mechanism remains unclear (26). However, little is known about the role of FGF10 in the pathogenesis of peritoneal fibrosis in PD. Hence, the results of our study provide a direct correlation between miR-145 and FGF10 in the pathogenesis of peritoneal fibrosis in PD *in vivo* and *in vitro*.

Results

miR-145 is elevated in TGF-β1–induced EMT in vitro and PD-induced peritoneal fibrosis in vivo

To determine the function of miR-145 in peritoneal fibrosis, we first determined whether there was a difference in the expression of miR-145 between normal cells and TGF-β1–induced HMrSV5 cells. Following stimulation with 10 ng/ml external TGF-β1 for different times (0, 12, 24, and 48 h), miR-145 expression was detected in HMrSV5 cells by RT-qPCR. We found that miR-145 was significantly up-regulated with longer stimulating times, and this effect became much more pronounced at 24 and 48 h (Fig. 1*A*). To further explore the plateau phase of miR-145 expression, we extended the stimulation time of TGF-β1 to 5 days and measured the miR-145 expression (Fig. S1*A*). Compared with 2 days, we discovered that the expression of miR-145 became higher at 3 days. There is no significant expression difference of miR-145 between 3 and 5 days. Therefore, the expression of miR-145 was considered to enter the plateau at 3 days.

Next, we detected changes in EMT-related indicators to verify the occurrence of peritoneal fibrosis in HMrSV5 cells. In general, the EMT process can be characterized using several biomarkers, among which fibronectin 1 (FN1) and α-smooth muscle actin (α-SMA) are acquired markers and E-cad is an attenuated marker. A previous study found that the expression of collagen I α 1 (Col1α1) was elevated during the EMT of HMrSV5 cells (17). In our study, after the stimulation with TGF-β1, the expressions of FN1, α-SMA, and Col1α1 (Fig. 1, *B* and *C*) increased and E-cad (Fig. 1*D*) decreased in HMrSV5 cells. However, the expression of EMT markers seemed only marginally affected by TGF-β1. To explore whether the EMT was successfully induced, cell morphology was shot, and the E-cadherin localization and induction of EMT-inducing transcription factors (EMT-TFs) were examined by immunofluorescence.

E-cad is an epithelial gene whose loss is a hallmark of EMT. Cells lack of E-cad will show spindle-shaped mesenchymal morphology and a loss of polarity. The silencing and transcriptional repression of E-cad during EMT is mediated by EMT-TFs, which contain the Snail (Snail1 and Snail2), Zeb (ZEB1 and ZEB2), and basic helix-loop-helix (bHLH and TWIST) families (27, 28). After stimulating with TGF-β1 for 48 h, we found that the cells lost the original paving stone shape and gained the spindle-shaped mesenchymal morphology feature (Fig. S1*B*). We then further examined the HMrSV5 cells using immunofluorescence. We discovered that the E-cad protein was located mainly on the cell membrane. After TGF-β1 stimulation, the protein level and localization of E-cad trended lower, whereas ZEB1 nuclear translocation was enhanced. The Western blotting examination of ZEB1 expression also showed an upward trend after TGF-β1 stimulation. Thus, we are convinced that TGF-β is an effective factor to induce EMT in HMrSV5 cells (Fig. S1, *C–E*).

We then examined the sequential events in miR-145, α-SMA, and FGF10 per 3 h using RT-qPCR when the cells were stimulated by TGF-β in the time interval between 12 and 24 h. As a result, miR-145 showed a significant increase at 15 h. After

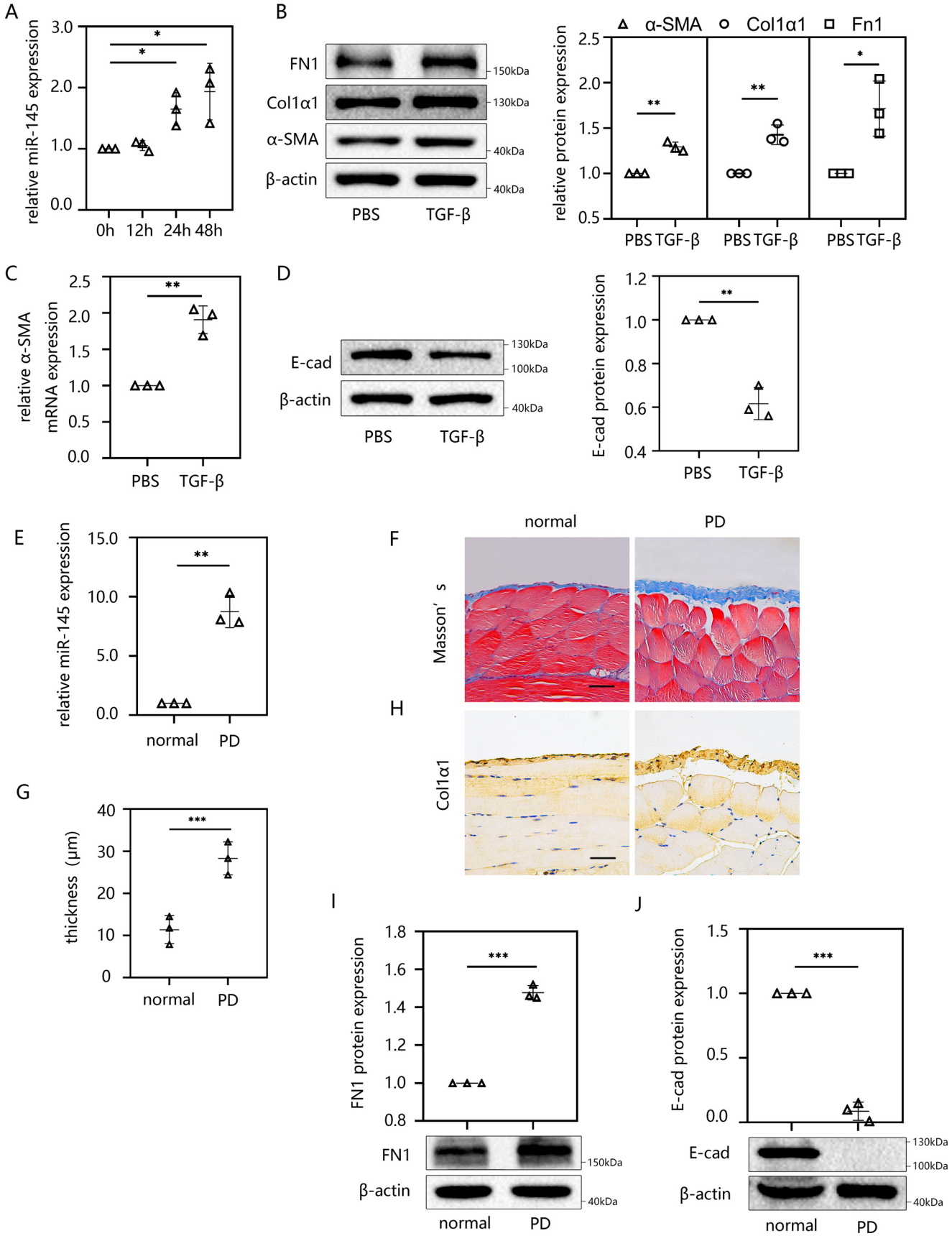
A
relative miR-145 expression
3.0
2.0
1.0
0.0
*
*
0h 12h 24h 48h
B
FN1
Col1α1
α-SMA
β-actin
150kDa
130kDa
40kDa
40kDa
PBS TGF-β
α-SMA Col1α1 Fn1
relative protein expression
2.5
2.0
1.5
1.0
0.5
**
**
*
PBS TGF-β PBS TGF-β PBS TGF-β
C
relative α-SMA mRNA expression
2.5
2.0
1.5
1.0
0.5
0.0
**
PBS TGF-β
D
E-cad
β-actin
130kDa
100kDa
40kDa
PBS TGF-β
E-cad protein expression
1.2
1.0
0.8
0.6
0.4
**
PBS TGF-β
E
relative miR-145 expression
15.0
10.0
5.0
0.0
**
normal PD
F
normal PD
Masson' s
H
Col1α1
G
thickness (μm)
40
30
20
10
0
***
normal PD
I
FN1 protein expression
1.8
1.6
1.4
1.2
1.0
0.8
***
FN1
β-actin
150kDa
40kDa
normal PD
J
E-cad protein expression
1.5
1.0
0.5
0.0
***
E-cad
β-actin
130kDa
100kDa
40kDa
normal PD

3 h of that, FGF10 mRNA began to decrease, and the mRNA of α-SMA was decreased at 24 h (Fig. S1, *F–H*).

To determine whether a similar phenomenon occurred in an animal model, we developed a mouse model of peritoneal fibrosis by daily injecting mice with 4.25% peritoneal dialysis fluid (PDF) for 28 days. The expression of miR-145 in the visceral peritoneum was examined by RT-qPCR. The results showed that miR-145 was up-regulated significantly in the PD group compared with the level in normal mice (Fig. 1*E*). Next, we performed Masson's trichrome staining on the parietal peritoneum. The results showed that mice in the PD group developed a thicker fibrous layer of the peritoneum (Fig. 1, *F* and *G*). The expression of Col1α1 in PD mice was significantly increased according to the immunohistochemical staining (Fig. 1*H*). In Western blotting results, FN1 (Fig. 1*I*) expression increased, whereas E-cad (Fig. 1*J*) was down-regulated after PD processing. All of these results indicated that miR-145 plays a role in the development of peritoneal fibrosis.

Overexpression of miR-145 effectively induced EMT in HMrSV5 cells

We first demonstrated that the expression level of miR-145 increased in TGF-β1–stimulated HMrSV5 cells and PDF-induced mice. The up-regulation of miR-145 suggested that miR-145 might be involved in the regulation of EMT in peritoneal fibrosis. To further explore this role, HMrSV5 cells were transfected with miR-145 mimics, and the transfection efficacy was assessed using RT-qPCR. The results showed that miR-145 was significantly elevated in HMrSV5 cells after the transfection of miR-145 mimics (Fig. 2*A*). Then we determined whether the increase in miR-145 had an effect on peritoneal fibrosis. Immunofluorescence assays were performed to show the expression and localization of E-cad. As a result, we found that the cells treated with miR-145 mimics showed significantly weaker signals on the cell membrane compared with the control group (Fig. S2*A*). In addition, we had detected kinds of EMT-related indicators using RT-qPCR and Western blotting. It turned out that mesenchymally associated molecules (α-SMA and FN1) were up-regulated at the mRNA level (Fig. 2*C*) and that the protein expression of α-SMA, Col1α1, and FN1 increased (Fig. 2*B*), whereas the intercellular adhesion molecule E-cad was down-regulated following the overexpression of miR-145 (Fig. 2*D*). We also knocked down miR-145 by transfecting an miR-145 inhibitor into HMrSV5 cells (Fig. 2*E*). The RT-qPCR and Western blotting analyses revealed opposite results in the miR-145 mimic group: α-SMA and FN1 decreased at the mRNA (Fig. 2*F*) and α-SMA, Col1α1, and FN1 decreased at protein levels (Fig. 2*G*), whereas E-cad protein increased at the protein level by Western blotting (Fig. 2*H*) and immunofluorescence analysis (Fig. S2*A*). To determine whether miR-145 is downstream of TGF-β signal, we transfected HMrSV5 cells with control inhibitor or miR-145 inhibitor and then incubated the cells with TGF-β1 for 48 h. EMT markers and Snail1 were evaluated in the cells. The results showed that the expressions of EMT makers and Snail1 were altered by TGF-β1 in part (Fig. 2*B*). This illustrated that miR-145 is downstream of TGF-β1 signal, and TGF-β1-mediated EMT changes require the induction of miR-145. However, miR-145 might not be the only pathway that could induce fibrosis changes when stimulated by TGF-β1. In conclusion, overexpression of miR-145 promoted peritoneal fibrosis by inducing EMT in HMrSV5 cells.

FGF10 was suppressed in both in vitro and in vivo peritoneal fibrosis models: TGF-β1–induced HMrSV5 cells and PD-treated mice

FGF10 belongs to the FGF family. The overexpression of FGF10 can significantly attenuate both the inflammatory and fibrotic phases, resulting in lung fibrosis (26). Moreover, it has been reported that TGF-β1 inhibits FGF10 expression in lung fibroblasts (29); however, little is known about the role of FGF10 in peritoneal fibrosis. We first verified the expression of FGF10 in the pathogenesis of peritoneal fibrosis *in vitro* and *in vivo*. TGF-β1–induced EMT in HMrSV5 cells resulted in the marked down-regulation of FGF10 at both the mRNA (Fig. 3*A*) and protein levels (Fig. 3*B*). In an *in vivo* experiment, the expression of FGF10 was suppressed in PD-induced peritoneal fibrosis in mice at the mRNA (Fig. 3*C*) and protein levels (Fig. 3, *D* and *E*). Immunohistochemical staining of the parietal peritoneum of mice revealed a similar trend of FGF10 expression between PD-treated mice and the normal group (Fig. 3*F*). Taken together, we conclude that FGF10 may play a role in peritoneal fibrosis.

Knockdown of FGF10 induced the procession of EMT in HMrSV5 cells

In the next series of experiments, we determined whether FGF10 had an impact on peritoneal fibrosis and the effect of the absence of FGF10. To answer these questions, two different FGF10 siRNAs (si-FGF10s) and negative control siRNA were separately transfected into HMrSV5 cells, and the efficiency of knockdown was evaluated by RT-qPCR (Fig. 4*A* and Fig. S3*A*) and Western blotting (Fig. 4*B* and Fig. S3*B*). Then the peritoneal fibrosis in the si-FGF10 group was analyzed. The protein levels of FN1, Col1α1, and α-SMA were significantly increased compared with those in the control group (Fig. 4*C*), whereas the protein level of E-cad decreased markedly by Western blot analysis. (Fig. 4*D*). To determine whether FGF10 is down-

Figure 1. miR-145 is elevated in TGF-β1–induced EMT *in vitro* and PD-induced peritoneal fibrosis *in vivo*. The miR-145 expression level was determined by RT-qPCR. EMT and peritoneal fibrosis were detected by Masson's trichrome staining, immunohistochemistry, Western blotting, and RT-qPCR. *A*, miR-145 expression was examined in HMrSV5 cells treated with 10 ng/ml TGF-β1 for different times (0, 12, 24, and 48 h). *B–D*, HMrSV5 cells were starved for 12 h and then treated with 10 ng/ml TGF-β1. After 24 h, cells were harvested, and the protein levels of FN1, Col1α1, α-SMA (*B*), and E-cad (*D*) were evaluated by Western blotting. The mRNA level of α-SMA was evaluated by RT-qPCR (*C*). Male C57BL/6J mice were intraperitoneally injected daily with 3 ml of 4.25% dextrose PD solution for 4 weeks before the parietal and visceral peritoneum tissues were collected. *E*, the miR-145 expression level was analyzed by RT-qPCR. *F* and *G*, Masson's trichrome staining of anterior abdominal walls (*F*). *G*, thickness of the peritoneal membrane. *H*, immunohistochemistry was performed to analyze the expression of Col1α1 protein. *I* and *J*, Western blot analysis was used to detect the protein expression levels of FN1 (*I*) and E-cad (*J*). Each *bar* shows the mean ± S.D. (*error bars*) from three independent experiments. **, $p < 0.01$; ***, $p < 0.001$ *versus* the control group. *Scale bar*, 50 μm.

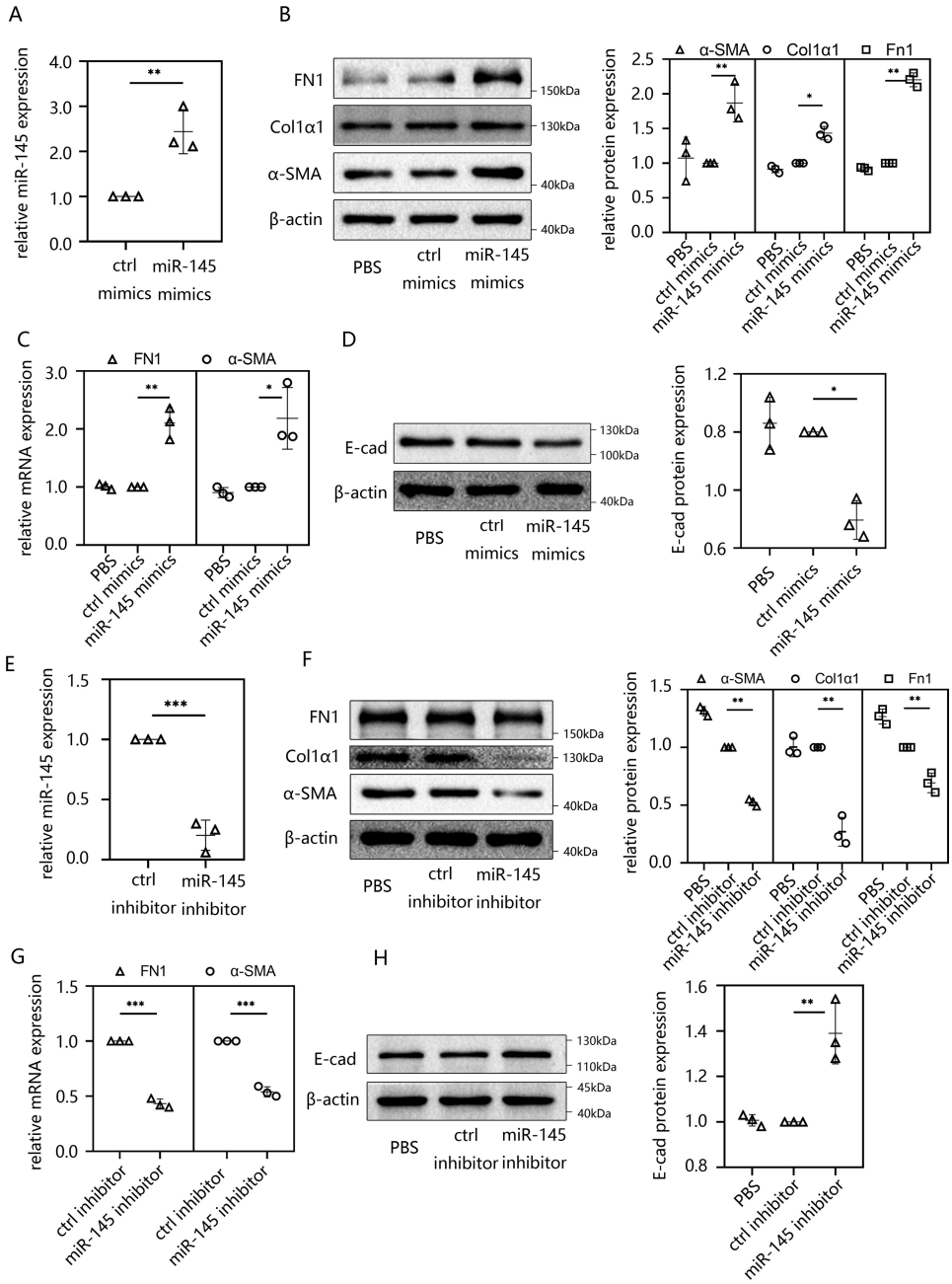

Figure 2. Overexpression of miR-145 effectively induced EMT in HMrSV5 cells. *A*, HMrSV5 cells were transfected with miR-145 mimics or ctrl mimics for 48 h. Then cells were harvested. The miR-145 expression level was analyzed by RT-qPCR. *B–D*, the protein expression levels of FN1, Col1α1, and α-SMA (*B*) and E-cad (*D*) were evaluated by Western blotting. The mRNA level of FN1 and α-SMA was evaluated by RT-qPCR (*C*). *E*, HMrSV5 cells were transfected with miR-145 inhibitor or ctrl inhibitor for 48 h before cells were harvested. The miR-145 expression level was analyzed by RT-qPCR. *F–H*, the protein expression levels of FN1, Col1α1, and α-SMA (*F*) and E-cad (*H*) were examined by Western blotting. The mRNA level of FN1 and α-SMA was evaluated by RT-qPCR (*G*). Data are presented as the mean ± S.D. (*error bars*) for three independent samples in each group. *, $p < 0.05$; **, $p < 0.01$; ***, $p < 0.001$ *versus* the control group.

stream of TGF-β signal, we transfected HMrSV5 cells with FGF10 siRNA or control siRNA for 24 h and then incubated the cells with 10 ng/ml TGF-β1 for 48 h. EMT markers, Snail1, and ZEB1 were evaluated by Western blotting. By comparing the si-FGF10 group with the NC group, we verified that both of the si-FGF10s induced EMT, and the EMT was slightly altered by additional TGF-β1 stimulation. However, there is no difference between TGF-β1 and si-FGF10+TGF-β1 group (Fig. S3, *C* and *D*), illustrating that although FGF10 is downstream of miR-145 and TGF-β1 signal, it may not be the only pathway of TGF-β1 that can induce fibrosis. These results are consistent with our previous findings.

miR-145 targeted the 3′-UTR of FGF10

It has been confirmed that microRNAs regulate protein translation by targeting the 3′-UTR region of mRNA (30). After finding that miR-145 can induce EMT and peritoneal fibrosis, we explored its downstream mechanism. We used the TargetScan online web servers (Whitehead Institute, Cambridge, MA) to predict the target mRNAs. The computational predictions

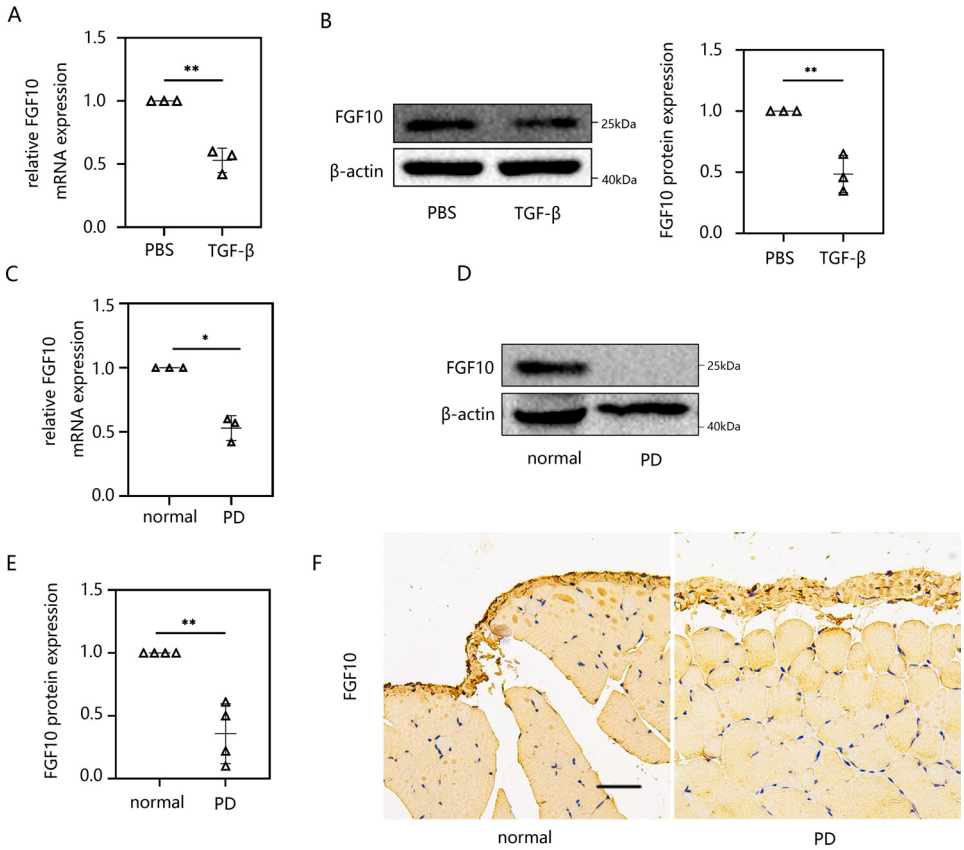

Figure 3. FGF10 was suppressed in both *in vitro* and *in vivo* peritoneal fibrosis models: TGF-β1–induced HMrSV5 cells and PD-treated mice. *A* and *B*, HMrSV5 cells were starved for 12 h and then treated with 10 ng/ml TGF-β1. After 24 h, cells were harvested. The expression levels of FGF10 mRNA (*A*) and protein (*B*) were evaluated using RT-qPCR and Western blot analysis. *C–E*, male C57BL/6J mice were intraperitoneally injected daily with 3 ml of 4.25% dextrose PD solution for 4 weeks before parietal and visceral peritoneum tissues were collected. The mRNA (*C*) and protein level (*D* and *E*) of FGF10 was analyzed by RT-qPCR and Western blotting. *F*, immunohistochemistry was performed to measure the FGF10 response. Data are presented as the mean ± S.D. (*error bars*) for three independent samples in each group. *, $p < 0.05$; **, $p < 0.01$ *versus* the control group. *Scale bar*, 50 μm.

revealed that the nucleic acid sequence of the highly conserved miR-145 contains binding sites on the 3′-UTR of FGF10 (Fig. 5*A*). To further confirm the interaction between miR-145 and FGF10, we transfected miR-145 mimics into HMrSV5 cells. The results indicated that the expression of FGF10 decreased at both the mRNA (Fig. 5*B*) and protein levels (Fig. 5*C*) compared with those in the control group. We then determined whether miR-145 and FGF10 mRNA underwent direct base pair binding. Luciferase reporters containing the full-length 3′-UTR (WT) of FGF10 or mutational vectors (mut) were constructed, and HMrSV5 cells were transiently transfected with the different reporters. The results indicated that cells cotransfected with miR-145 mimics reduced luciferase activity of WT 3′-UTR of FGF10 compared with that in cells transfected with control mimics (Fig. 5*D*).

miR-145 promoted EMT and peritoneal fibrosis by targeting FGF10 in HMrSV5 cells

As stated earlier, we found that both the overexpression of miR-145 and knockdown of FGF10 can induce EMT and peritoneal fibrosis. Then luciferase reporter assays confirmed a direct binding effect between miR-145 and FGF10 mRNA. These results prompted us to further determine whether knockdown miR-145 could promote the expression of FGF10. After miR-145 inhibitor transfection for 48 h, HMrSV5 cells were collected to detect the expression of FGF10. The experimental results revealed that both the mRNA (Fig. 6*A*) and protein levels (Fig. 6*B*) of FGF10 showed a significant upward trend compared with those in the control group. To confirm whether miR-145 promotes EMT and peritoneal fibrosis through FGF10, we transfected HMrSV5 cells with si-FGF10 and negative control siRNA for 48 h. Then the cells underwent a second transfection with miR-145 mimics or miR-145 inhibitor. Interestingly, there was no significant difference in fibrosis-related indicators, such as FN1, α-SMA, Col1α1 (Fig. 6*C*), and E-cad (Fig. 6*D*), between the two groups.

FGF10 treatment suppressed miR-145–induced EMT in peritoneal fibrosis

To further confirm the underlying anti-EMT effect of FGF10, we transfected HMrSV5 cells with miR-145 mimics for 48 h and then incubated the cells in medium containing 100 ng/ml human FGF10 for 24 h. The Western blotting results indicated that the increased expression levels of α-SMA and FN1 were reversed after FGF10 treatment (Fig. 7*A*). The decreased expression of E-cad showed a certain degree of recovery after FGF10 treatment (Fig. 7*B*) compared with that in the miR-145 mimics group. Additional FGF10 treatment can decrease the expression of α-SMA compared with the

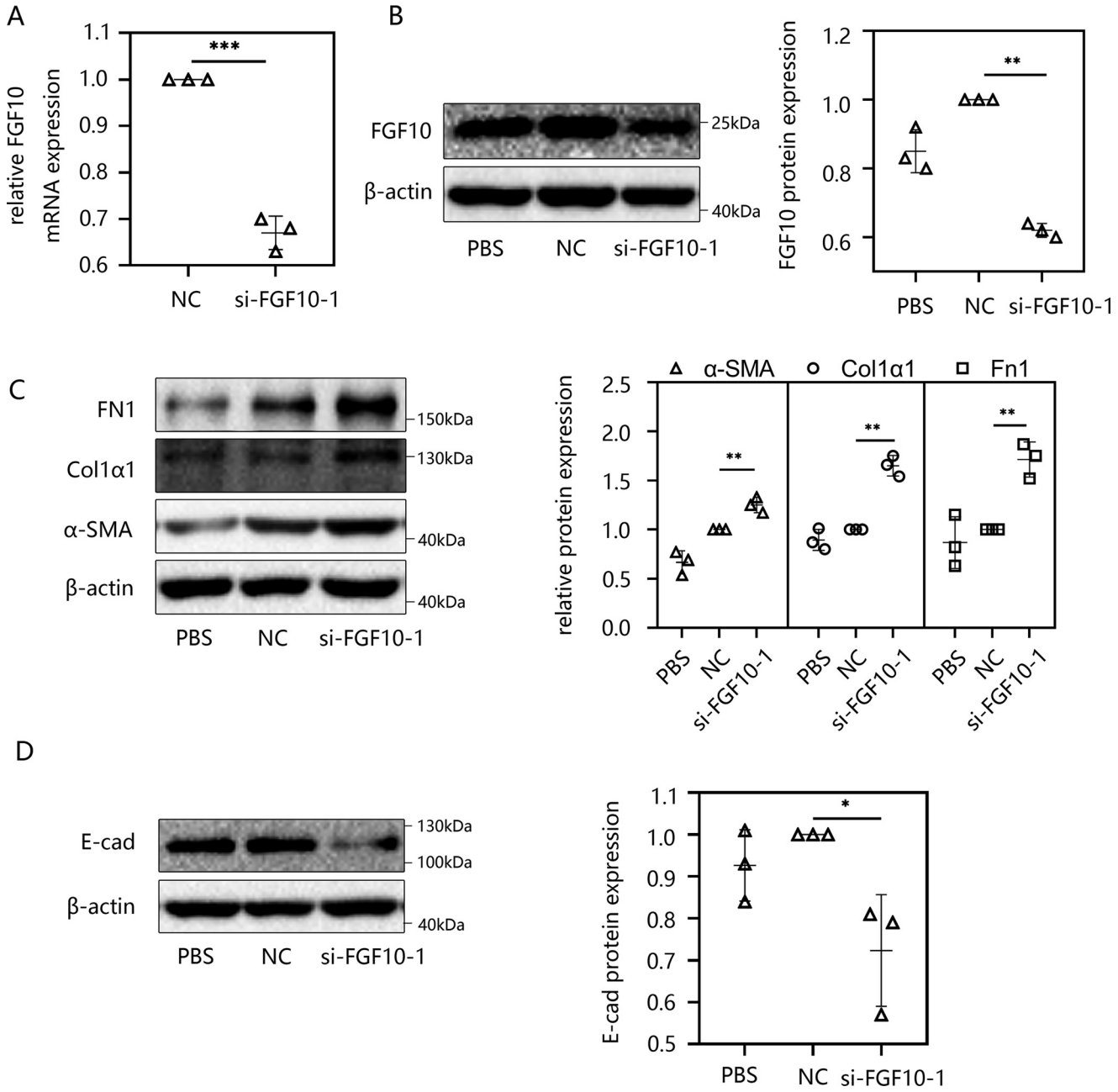

Figure 4. Knockdown of FGF10 induced the procession of EMT in HMrSV5 cells. *A* and *B*, HMrSV5 cells were transfected with negative control siRNA or si-FGF10. After 48 h, cells were harvested, and the transfection efficacy was analyzed by RT-qPCR (*A*) and Western blotting (*B*). *C* and *D*, HMrSV5 cells were transfected with negative control siRNA or si-FGF10. After 48 h, cells were harvested. Western blot analysis was used to detect the protein levels of FN1, Col1α1, and α-SMA (*C*) and E-cad (*D*). Data are presented as the mean $\pm$ S.D. (*error bars*). *, $p < 0.05$; **, $p < 0.01$; ***, $p < 0.001$ *versus* the NC group.

control (ctrl) mimic group (Fig. S4*B*). Previous research discovered that TGF-β1–induced EMT accompanies IIIb-to-IIIc isoform switching of FGFR (31), whereas FGF10 only acts on the IIIb receptor. This phenomenon leads to the insensitivity of cells to FGF10 stimulation. So we are very curious why FGF10 treatment could still relieve peritoneal fibrosis after transfection of miR-145. Thus, HMrSV5 cells were transfected with miR-145 mimics for 48 h. FGFR2IIIb expression was examined by conventional RT-PCR. We found that FGFR2IIIb was only slightly decreased compared with control group. The effect of isoform switching may be resisted by extra FGF10 treatment (Fig. S4*C*). To further explore whether miR-145 has an effect on EMT, we increased the concentration of miR-145 mimics used for transfection. We used 50, 100, and 200 nM miR-145 mimics to transfect cells, respectively. As a result, E-cad was suppressed to a greater extent compared with other groups (Fig. S4*E*). This demonstrated that miR-145 can indeed inhibit the expression of E-cad and promote EMT, and as it increased in HMrSV5 cells, the effect tended to be more pronounced. Taken together, these results suggested that miR-145 can induce EMT and that FGF10 has an inhibitory effect on peritoneal fibrosis.

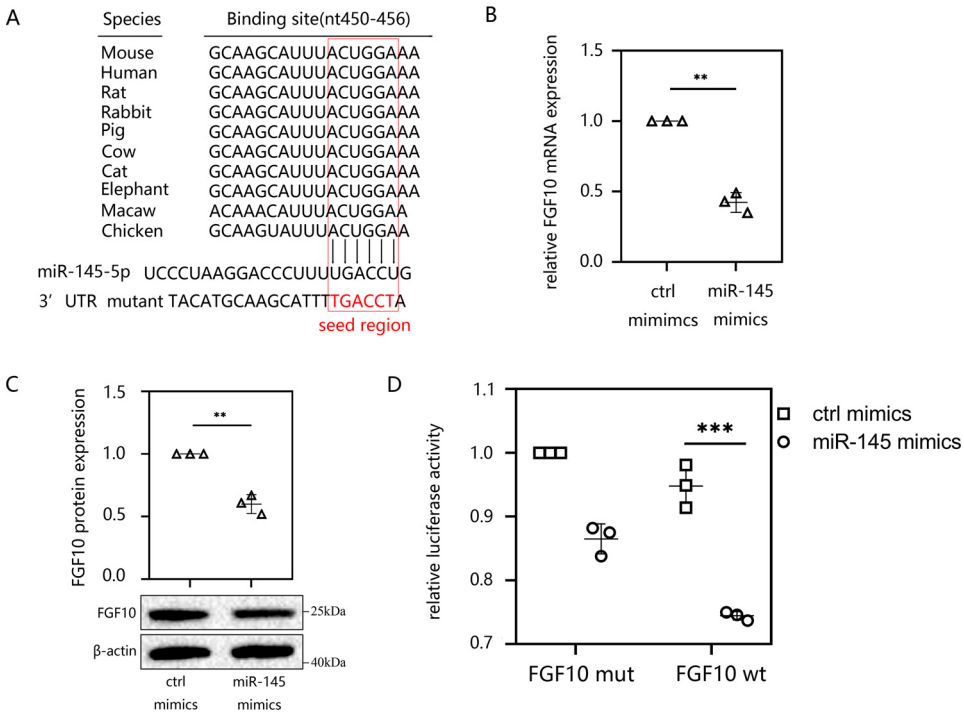

Figure 5. miR-145 targeted the 3′-UTR of FGF10. *A*, using the TargetScan database, the nucleic acid sequence of miR-145-5p was predicted to contain binding sites for the 3′-UTR of FGF10 in different species. *B* and *C*, HMrSV5 cells were transfected with miR-145 mimics or ctrl mimics for 48 h. The mRNA (*B*) and protein levels (*C*) of FGF10 were analyzed by RT-qPCR and Western blotting. *D*, luciferase activity of HMrSV5 cells transfected with a luciferase reporter containing the WT or mutated 3′-UTR of FGF10. Then cells were cotransfected with miR-145 mimics or ctrl mimics, and the normalized levels of luciferase activity are shown. The results are presented as the mean ± S.D. (*error bars*) from three independent experiments. The -fold change is statistically significant. *, $p < 0.05$; **, $p < 0.01$; ***, $p < 0.001$.

Exogenous delivery of miR-145 promoted peritoneal fibrosis in an established PD model in vivo

We then determined the functional role of miR-145 *in vivo*. First, the transfection efficiency of miR-145 mediated by ultrasonic microbubbles was determined by RT-qPCR. The results showed that the PD mice treated with the miR-145 expression plasmid exhibited significantly increased expression of miR-145 in the peritoneal tissue compared with that in the control group. In contrast, in PD mice, the miR-145 shRNA plasmid exhibited a strong inhibitory effect on miR-145 in the peritoneum (Fig. 8*A*). Then we examined the peritoneal fibrosis by Masson's trichrome staining (Fig. 8*B*). The results showed that the PD mice had thicker matrix deposition compared with the normal group. This demonstrates that our peritoneal fibrosis model was successfully developed. We also observed that the peritoneal fibrosis caused by PD was further aggravated by the miR-145 expression plasmid. Mice that underwent PD and overexpression of miR-145 had the thickest peritoneal fibrous layer among the five groups. However, in the group transfected with the miR-145 shRNA plasmid, fibrosis was significantly reduced compared with that in the NC group (Fig. 8*C*). Accordingly, these histological changes were associated with the change in peritoneal function determined by modified peritoneal equilibration tests. Based on the statistical results, the thickening of the peritoneal fibrous layer in the miR-145 expression plasmid group was related to the increased efficiency of solute transport compared with that in the NC group, which was characterized by a decrease in D/D_0. In contrast, miR-145 knockdown alleviated the peritoneal dysfunction caused by peritoneal fibrosis (Fig. 8*D*).

Overexpression of miR-145 aggravated peritoneal fibrosis in vivo as determined by RT-qPCR, Western blotting, and immunohistochemistry

Overexpression of miR-145 resulted in the gain of Col1α1 (Fig. 9*A*) and a significant loss of FGF10 (Fig. 9*B*) compared with levels in the NC group according to immunohistochemical staining of the wall peritoneum. In the visceral peritoneum, after transfecting miR-145 expression plasmid, FGF10 was decreased at the mRNA level (Fig. 9*C*). There were also increasing trends in the mRNA (Fig. 9*D*) and protein levels (Fig. 9*E*) of mesenchymal markers (α-SMA, FN1, and Col1α1) and a loss of the epithelial marker E-cad (Fig. 9*F*) after overexpressing miR-145. miR-145 knockdown attenuated peritoneal fibrosis, which suggests that it is a potential therapeutic target. The increase in α-SMA and Col1α1 caused by PD was reversed, and E-cad and FGF10 returned to normal levels following miR-145 knockdown.

Discussion

EMT can be divided into three general subtypes, among which the type 2 EMT is involved in the response to persistent inflammation and ultimately the induction of fibrosis (32). This process involves profound epithelial cell plasticity and is a reversible cellular program that transiently places epithelial cells into quasi-mesenchymal cell states (33, 34). In this process, the cells gradually lose polarity and adhesiveness and, finally,

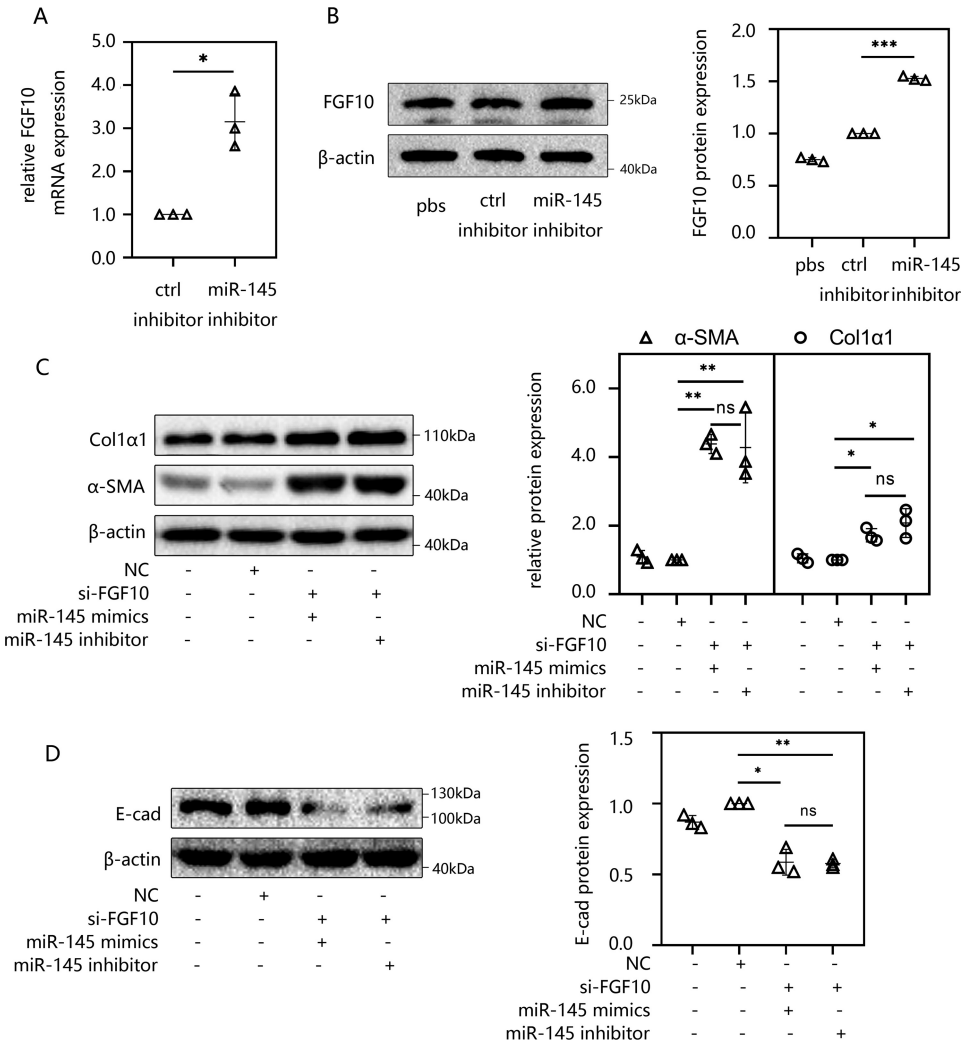

Figure 6. miR-145 promoted EMT and peritoneal fibrosis by targeting FGF10 in HMrSV5 cells. *A* and *B*, HMrSV5 cells were transfected with miR-145 inhibitor. After 48 h, cells were harvested. The mRNA levels (*A*) and protein levels (*B*) of FGF10 were determined by RT-qPCR and Western blotting. *C* and *D*, HMrSV5 cells were transfected with si-FGF10 for 48 h before a second transfection of miR-145 mimics or an inhibitor for 48 h. Then cells were harvested, and the protein levels of FN1, Col1α1, α-SMA (*C*), and E-cad (*D*) were analyzed by Western blotting. The results are presented as the mean $\pm$ S.D. (*error bars*) from three independent experiments. The -fold change is statistically significant. *, $p < 0.05$; **, $p < 0.01$; ***, $p < 0.001$.

become migratory by gaining mesenchymal characteristics while progressively losing epithelially associated markers, such as E-cad (35). In particular, there is emerging evidence of EMT being associated with the pathogenesis of peritoneal fibrosis (36). It has been demonstrated that EMT is one of the earliest mechanisms of peritoneal fibrosis, and MCs are known to undergo EMT to become matrix-producing myofibroblasts under pathologic conditions and participate in the pathogenesis of peritoneal fibrosis (37–39). The molecular mechanisms underlying EMT and fibrosis in the peritoneum may also be involved in clinical issues that are not related to PD, such as the prevention of postoperative peritoneal adhesions and control of peritoneal metastasis (40). MCs do not remain unchanged during the clinical process of PD treatment, and during its course, the cellular processes of EMT play a complex role in the acute cellular stress response and cytoresistance of MCs (41). Actually, TGF-β1 has been shown to play a significant role in the initiation and development of EMT as well as peritoneal fibrosis (42–44). It has been demonstrated that maternal exposure to di-*n*-butyl phthalate induces the accumulation of TGF-β1 in the kidneys and regulates Snail1-mediated EMT of tubular epithelial cells, which can strongly mediate EMT (45). In this study, we also determined that EMT was obviously activated in TGF-β1–stimulated HMrSV5 cells and in an established PD model *in vivo*. In fact, the pharmacological prevention and/or reversal of EMT may represent a possible therapeutic approach to peritoneal fibrosis; for example, intraperitoneal metformin decreases EMT and increases the ratio of reduced to oxidized GSH and SOD expression, whereas it decreases the expression of nitrotyrosine and 8-hydroxy-2′-deoxyguanosine (46).

Increasing evidence has demonstrated that miRNAs play pivotal roles in the pathogenesis of peritoneal fibrosis in PD, and miR-145 is of significant interest because it is up-regulated by TGF-β in fibrotic diseases (11, 18, 19). However, there are significant differences in gene expression among fibroblasts from different internal organs or dermal fibroblasts (47). For example, it has been reported that miR-145 was down-regulated in cardiac fibrosis as well as in keloid fibroblasts (48). Nonetheless, whether miR-145 can regulate peritoneal fibrosis

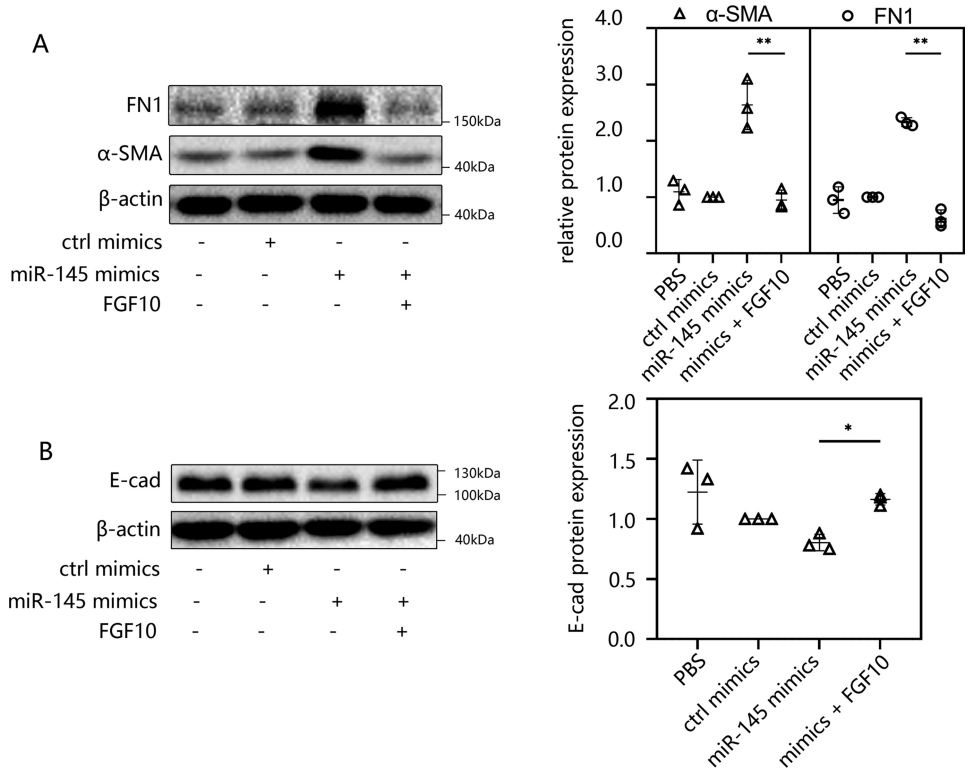

Figure 7. FGF10 treatment suppressed miR-145–induced EMT in peritoneal fibrosis. *A* and *B*, HMrSV5 cells were transfected with miR-145 mimics for 48 h, and then the cells were incubated in medium containing 100 ng/ml human FGF10 for 24 h. The cells were then harvested, and the levels of FN1 and α-SMA (*A*) and E-cad (*B*) were analyzed by Western blotting. The results are presented as the mean ± S.D. (*error bars*) from three independent experiments. The -fold change is statistically significant. *, $p < 0.05$; **, $p < 0.01$.

and the underlying mechanism remains unknown. We then hypothesized that the increased expression of miR-145 may be necessary for the progression of EMT and the pathogenesis of peritoneal fibrosis in PD. Therefore, we assessed the potential role of miR-145 in both TGF-β1–induced cell lines and a preclinical mouse model of peritoneal fibrosis. In our study, we found that miR-145 was up-regulated in the TGF-β1–stimulated HMrSV5 cells in a time-dependent manner, and the same trend was also found in the mouse model of PD-induced peritoneal fibrosis. Interestingly, this expression trend of miR-145 was consistent with the extent of EMT, indicating that the abnormal expression of miR-145 may be involved in the pathogenesis of peritoneal fibrosis. Moreover, transfection with miR-145 mimics in HMrSV5 cells could promote peritoneal fibrosis in HMrSV5 cells. In addition, our data on miR-145 gene transfer showed the same trend in an established PD model, which was highly consistent with the *in vitro* experiments. Consequently, these data indicate that the overexpression of miR-145 could effectively promote EMT and peritoneal fibrosis *in vitro* or *in vivo*.

FGF10, a multifunctional mesenchymal-epithelial signaling growth factor (21), was identified as a target of miR-145 in our study and decreased in TGF-β1–stimulated HMrSV5 cells, and the same trend regarding the expression of FGF10 was found in an established PD mouse model. Recent studies have shown that FGF10 reduces bleomycin-induced lung fibrosis (25); however, little is known about the role of FGF10 in the pathogenesis of peritoneal fibrosis in PD. Thus, combined with the results stated above, it is possible that FGF10 may play an inhibitory role in the pathogenesis of peritoneal fibrosis. To further clarify the role of FGF10 in the pathogenesis of peritoneal fibrosis, we knocked down the expression of FGF10 via transfecting si-FGF10 into HMrSV5 cells. Interestingly, the results indicated that the expression levels of α-SMA, Col1α1, and FN1 markedly increased, whereas that of E-cad was decreased following the transfection, meaning that knocking down the expression of FGF10 could significantly induce the process of EMT. Moreover, we found that the transfection of miR-145 mimics into HMrSV5 cells decreased FGF10 expression *in vitro*, supporting the targeting of FGF10 by miR-145 already demonstrated in the luciferase reporter assay in our study. Then we treated mice with PDF and found decreased expression levels of FGF10 in the peritoneal tissues, whereas we observed a similar result when silencing the FGF10 gene, in which FGF10 expression was also reduced by the up-regulation of miR-145 *in vivo*. Therefore, our data indicate that FGF10 is a target of miR-145. Correspondingly, we considered that the decreased expression of FGF10 was a sign of peritoneal fibrosis.

Conclusion

In conclusion, we found that TGF-β1 can induce peritoneal fibrosis by enhancing EMT, that the expression of miR-145 was up-regulated in TGF-β1–stimulated HMrSV5 cells, and that the overexpression of miR-145 promoted EMT by targeting FGF10. Moreover, knocking down the expression of FGF10 significantly accelerated the process of EMT. Furthermore, we found that FGF10 expression was markedly reduced by the up-

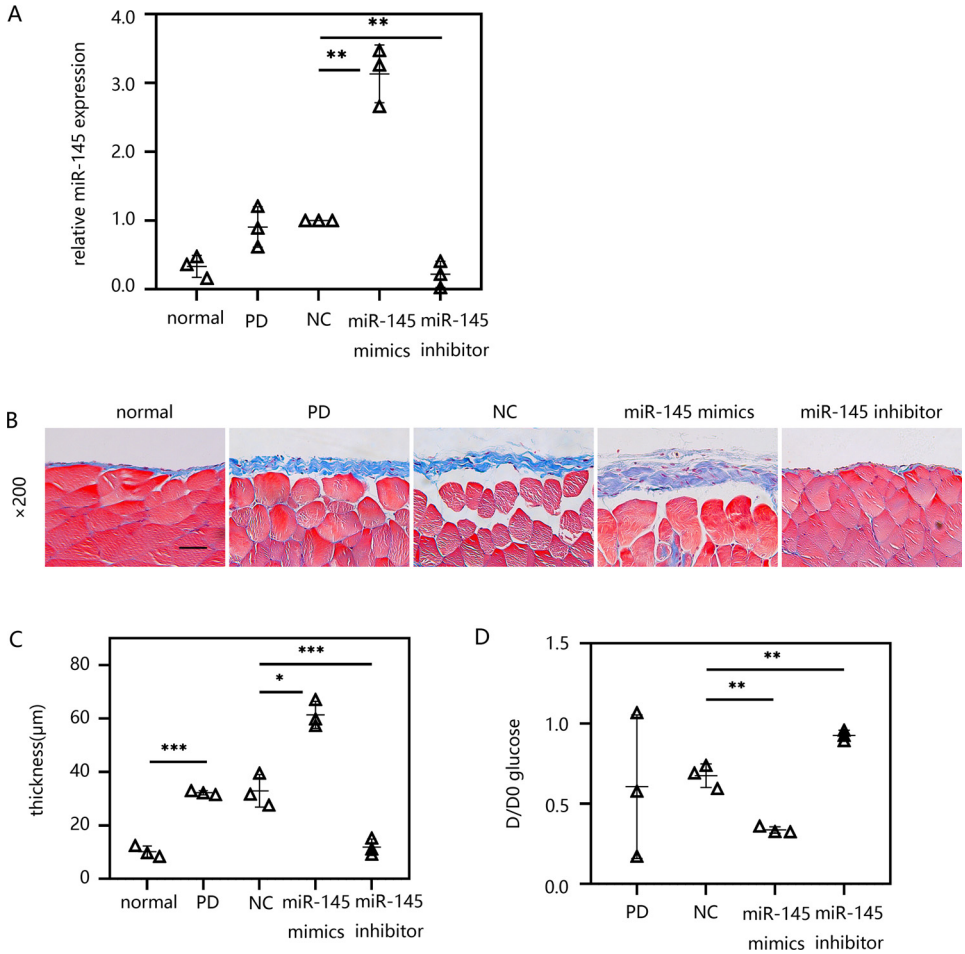

Figure 8. Exogenous delivery of miR-145 promoted peritoneal fibrosis in an established PD model *in vivo*. Male C57BL/6J mice were intraperitoneally injected daily with 3 ml of 4.25% dextrose PD solution for 4 weeks with/without treatment with ultrasound-microbubble-miR-145 mimic/inhibitor/NC plasmid on days 0 and 14. After 28 days of PDF treatment, the mice were killed. Both parietal and visceral peritoneal tissues were collected. *A*, the miR-145 expression level in the visceral peritoneum was evaluated by RT-qPCR. *B*, Masson's trichrome staining was performed on the anterior abdominal walls. *C*, the thickness of the peritoneal membrane was analyzed. *D*, peritoneal function was investigated by the transfer of glucose (D/D_0). The results are presented as the mean ± S.D. (*error bars*) from three independent experiments. The -fold change is statistically significant. *, $p < 0.05$; **, $p < 0.01$; ***, $p < 0.001$. *Scale bar*, 50 μm.

regulation of miR-145 *in vivo*. Taken together, our data suggest that miR-145 promotes EMT and peritoneal fibrosis by targeting FGF10 in the pathogenesis of peritoneal fibrosis in PD and implicate miR-145 as a potential therapeutic target for regulating peritoneal fibrosis in PD.

Materials and methods

Animal model

Male C57BL/6J mice (8–10 weeks old) were purchased from the Jinan Pengyue Laboratory Animal Breeding Co. Ltd. All experimental procedures and animal care were approved by the Southern Medical University Ethics Committee. The mice were randomly divided into five groups ($n = 10$). They were kept in a controlled environment and provided rodent chow and water. Investigators were blinded to the experimental treatments. To develop the mouse model, the mice were intraperitoneally injected daily with 3 ml of 4.25% dextrose PD solution (Baxter HealthCare, Deerfield, IL) for 4 weeks. Based on previous studies (42), we gave the mice ultrasound-microbubble-plasmid treatment on days 0 and 14 over 28 days. The five groups of mice were treated as follows: the normal group was fed without any treatment, mice in the PD group received daily intraperitoneal injections of 3 ml of 4.25% dextrose PDF for 4 weeks, and the three other groups received both PDF and ultrasound-mediated miR-145 mimic/inhibitor/control plasmid gene transfer treatment. After the 28-day PDF treatment, the mice were killed. The visceral peritoneal tissues were collected and stored at −80 °C for Western blotting and RT-qPCR. The anterior abdominal wall was fixed in 4% paraformaldehyde solution for Masson's trichrome staining and immunohistochemistry.

Modified peritoneal equilibration test

Modified peritoneal equilibration tests were performed to measure the ratio of glucose in the peritoneal dialysate and determine the type of peritoneal solute transport. Before being killed, the mice were intraperitoneally injected with 3 ml of 4.25% dextrose PDF. Two hours later, dialysate samples were collected. The concentrations of glucose in the dialysate were measured using an automated chemistry analyzer (Chemray240, Rayto, Shenzhen, China). We used D/D_0 to represent glucose transport efficiency, where D is the glucose concentration in the 2-h PDF solution, and D_0 is the

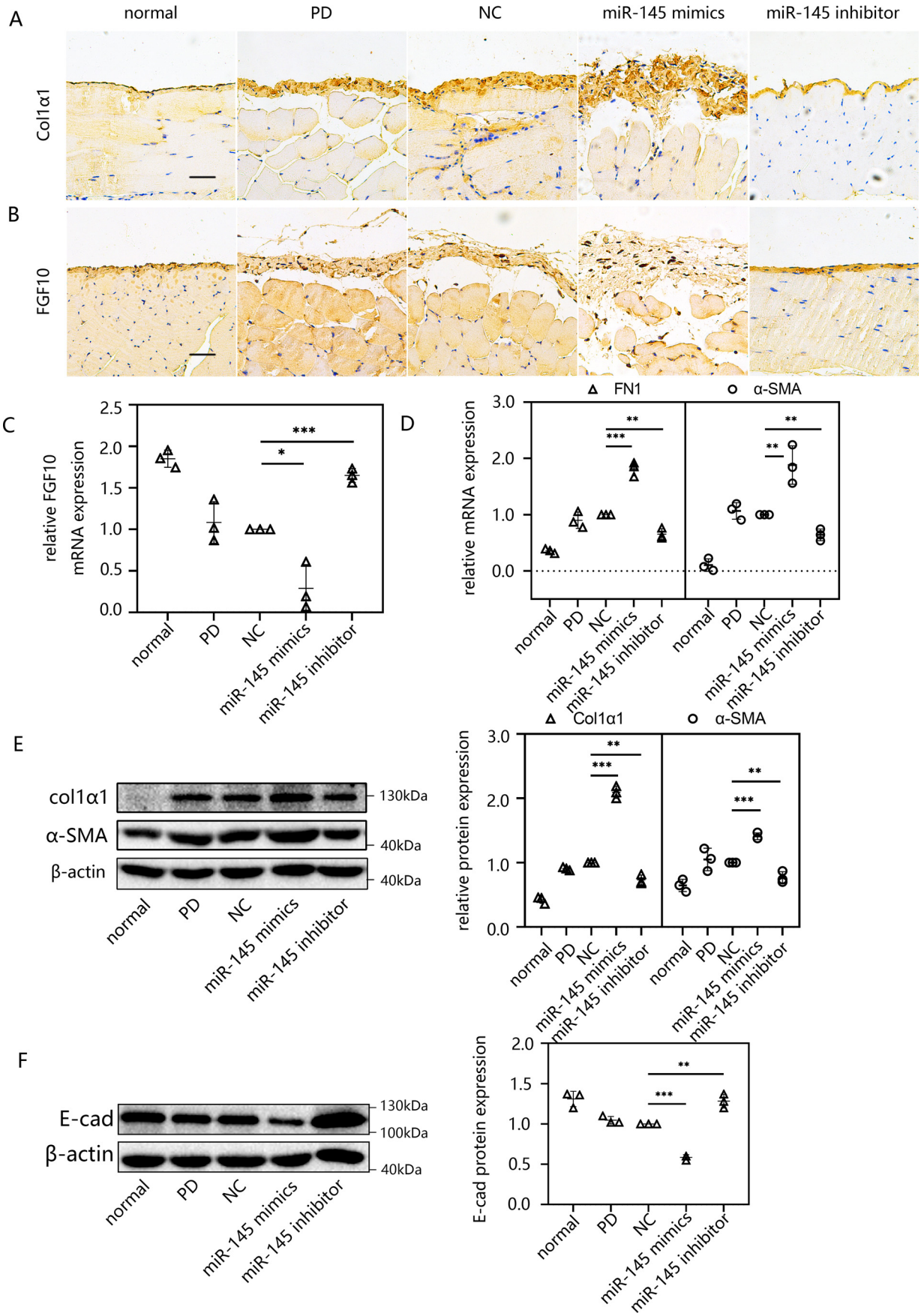
A
normal
PD
NC
miR-145 mimics
miR-145 inhibitor
Col1α1
B
FGF10
C
relative FGF10 mRNA expression
2.5
2.0
1.5
1.0
0.5
0.0
***
*
normal
PD
NC
miR-145 mimics
miR-145 inhibitor
D
FN1
α-SMA
relative mRNA expression
3.0
2.0
1.0
0.0
**
***
**
**
E
col1α1
α-SMA
β-actin
130kDa
40kDa
40kDa
Col1α1
α-SMA
relative protein expression
3.0
2.0
1.0
0.0
**
***
**
***
F
E-cad
β-actin
130kDa
100kDa
40kDa
E-cad protein expression
2.0
1.5
1.0
0.5
0.0
**
***

glucose concentration of PDF before instillation into the abdominal cavity.

Transfer of the miR-145 gene into the peritoneum via an ultrasound-microbubble–mediated system

We used the mmu-miR-145–5p overexpression plasmid to overexpress miR-145 in peritoneal tissue. The mmu-miR-145–5p shRNA plasmid was used to suppress miR-145 expression, and the ShNC vector was used as a control. The sequences of the three plasmid insertion regions are shown in Sequence S2–4. Three kinds of plasmid were designed by the GenePharma Company (Shanghai, China) and amplified using the GoldHi EndoFree Plasmid Maxi Kit (CW2104M, CWBIO, Beijing, China) according to the manufacturer's instructions. Three types of plasmid (miRNA-mmu-145-5p mimic, miRNA-mmu-145-5p inhibitor sponge, and ShNC vector) were each mixed with sulfur hexafluoride microbubbles (SonoVue, Bracco Diagnostics, Princeton, NJ) at a ratio of 1:1 (v/v). Then the mixture containing 200 μg of plasmid in a total volume of 1 ml was injected into the abdominal cavity of mice. We then applied the ultrasound probe (Sonitron 2000; Rich-Mar Corp., Inola, OK) vertical to the anterior surface of the abdominal skin coated with ultrasound media. A pulse wave at 1 MHz input frequency and 2 watt/cm^2 output intensity was applied to the entire anterior abdominal wall to guide the ultrasound microbubbles to reach the whole peritoneum.

Cell culture and treatment

HMrSV5 cells were obtained from the Key Laboratory of Nephrology in the First Affiliated Hospital of Sun Yat-Sen University (Guangzhou, China). Cells were maintained in Dulbecco's modified Eagle's medium/F-12 culture medium (Gibco) containing 10% heat-inactivated fetal bovine serum (Gibco) and incubated at a constant temperature of 37 °C in a humidified incubator with 5% CO_2. Before treatment with 10 ng/ml TGF-β1 (R&D Systems, Minneapolis, MN), the HMrSV5 cells were incubated without fetal bovine serum for 12 h. The characteristics of the HMrSV5 cell line have been described in previous studies (49).

RNA transfection

miR-145 mimics (miR10000437), control miRNA mimics (ctrl mimics) (miR01101), miR-145 inhibitor (miR20000437), and control miR-145 inhibitor (ctrl inhibitor) (miR2N0000001-1-5) were designed and synthesized by RiboBio (Guangzhou, China). The sense strand sequence of miRNA-145 mimics was 5′-GUCCAGUUUUCCCAGGAAUCCCU-3′, and the antisense strand sequence was 3′-CAGGUCAAAAGGGUCCUU-AGGGA-5′. The miR-145 inhibitor sequence was 5′-AGG-GAUUCCUGGGAAAACUGGAC-3′. The si-FGF10–1 and negative control siRNA were constructed by Shanghai GenePharma (Shanghai, China). The sequence of the sense strand of si-FGF10–1 was 5′-CGCUGGAGAAAGCUAUUCUTT-3′, and the antisense strand sequence was 5′-AGAAUAGCUUU-CUCCAGCGTT-3′. The siFGF10-2 was designed by RiboBio (siQ0001). Its target sequence was 5′-ACCTATGCATCATT-TAACT-3′. A specific RNA fragment was transfected into HMrSV5 cells using Lipofectamine 2000 Reagent (11668019; Invitrogen) at the recommended concentration (miR-145 mimic, 50 nM; miR-145 inhibitor, 100 nM; si-FGF10, 100 nM) according to the manufacturer's instructions.

Table 1
Primer sequences used in RT-qPCR
The forward and reverse primer sequences of human α-SMA, human FN1, human FGF10, human β-actin, GAPDH, human FGFR2IIIb, mouse α-SMA, mouse FN1, mouse FGF10, and mouse β-actin were applied in this study.

Gene	Primer sequences
Humanα-SMA	
Forward	5′-CAGCAGATGTGGATCACCAAGCAG-3′
Reverse	5′-CCATTGAGAAGATTCGTCGTCCTGAG-3′
Human FN1	
Forward	5′-GAGAATAAGCTGTACCATCGCAA-3′
Reverse	5′-CGACCACATAGGAAGTCCCAG-3′
Human FGF10	
Forward	5′-CGGCTGCTGCTGCTGCTG-3′
Reverse	5′-AGGAGAAGGAGGAGGAAGAAGAGTTG-3′
Human β-actin	
Forward	5′-CATGTACGTTGCTATCCAGGC-3′
Reverse	5′-CTCCTTAATGTCACGCACGAT-3′
Human GAPDH	
Forward	5′-GGCACCGTCAAGGCTGAGAAC-3′
Reverse	5′-GGTGGCAGTGATGGCATGGAC-3′
Human FGFR2IIIb	
Forward	5′-CACTCGGGGATAAATAGTT-3′
Reverse	5′-ACTCGGAGACCCCTGCCA-3′
Mouse α-SMA	
Forward	5′-GTCCCAGACATCAGGGAGTAA-3′
Reverse	5′-TCGGATACTTCAGCGTCAGGA-3′
Mouse FN1	
Forward	5′-GATGTCCGAACAGCTATTTACCA-3′
Reverse	5′-CCTTGCGACTTCAGCCACT-3′
Mouse FGF10	
Forward	5′-TGCTCTTCTTCCTCCTCGTCCTTC-3′
Reverse	5′-CCGCTGACCTTGCCGTTCTTC-3′
Mouse β-actin	
Forward	5′-GTGACGTTGACATCCGTAAAGA-3′
Reverse	5′-GCCGGACTCATCGTACTCC-3′

RNA extraction and RT-PCR

Total RNA was isolated from cells or peritoneal tissues of mice with TRIzol reagent (Takara, Dalian, China) according to the manufacturer's instructions. Then a reverse transcription kit (RR047A, Takara) was used for the reverse transcription of total RNA into cDNA. Afterward, the relative expression of mRNA was determined by real-time fluorescent quantitative PCR using SYBR Premix Ex Taq™ II (RR820A, Takara) according to the manufacturer's instructions, and the amplified product was used in conventional RT-PCR. Primer pairs for the detection of human β-actin and glyceraldehyde-3-phosphate dehydrogenase (GAPDH) are used as the internal control (Table 1). miR-145–specific PCR primers (MQP-0101, RiboBio) were used for the reverse transcription of miR-145 fol-

Figure 9. Overexpression of miR-145 aggravated peritoneal fibrosis *in vivo*, as determined by RT-qPCR, Western blotting, and immunohistochemistry. *A* and *B*, immunohistochemistry was applied to assess the expression of Col1α1 (*A*) and FGF10 (*B*) in the anterior abdominal walls. *C* and *D*, the mRNA levels of FGF10 (*C*) and FN1 and α-SMA (*D*) were determined by RT-qPCR. *E* and *F*, Western blotting confirmed the expression of FN1, α-SMA, and Col1α1 (*E*) and E-cad (*F*). The results are presented as the mean ± S.D. (*error bars*) from three independent experiments. The -fold change is statistically significant. *, $p < 0.05$; **, $p < 0.01$; ***, $p < 0.001$. *Scale bar*, 50 μm.

lowed by normalization to U6 snRNA (MQP-0201, RiboBio). The RT-qPCR kit for miR-145 was the same as that mentioned above. The relative quantification of each gene was calculated and normalized using the $2^{-\Delta\Delta Ct}$ method.

Western blot analysis

A Western blotting assay was performed to measure proteins in cells and peritoneal tissues. Total protein was lysed with radioimmune precipitation assay lysis buffer (P0013B, Beyotime, Jiangsu, China) containing 1% phenylmethylsulfonyl fluoride following the manufacturer's protocol. The protein concentration was measured with a bicinchoninic acid (BCA) protein assay (P011, GeneCopoeia Inc., Rockville, MD) before denaturing at 99 °C for 5 min. Then the protein solution was subjected to SDS-PAGE and transferred to a nitrocellulose membrane (pore size 0.45 μm; Millipore). After blocking the membrane in 5% skimmed milk in TBS-Tween (20 mM Tris-HCl, 150 mM NaCl, and 0.1% Tween 20) for 1 h at room temperature, the membrane was then incubated with primary antibody at 4 °C overnight. The antibodies used in this study were as follows: mouse anti-β-actin (1:5000; E021020-02, Earthox), rabbit anti-FN1 (1:5000; ab2413, Abcam, Cambridge, MA), mouse anti-E-cad (1:2500; BD Biosciences), rabbit anti-Col1α1 (1:200; BA0325, Boster Bio-engineering Ltd. Co., Wuhan, China), rabbit anti-α-SMA (1:1000; ab5694, Abcam), rabbit anti-FGF10 (1:2000; 345-FG-025, R&D Systems, Minneapolis, MN), rabbit anti-Snail1 (1:1000; AF6032, Affinity Biosciences), and rabbit anti-ZEB1 (1:500; DF7414, Affinity Biosciences). The membrane was washed in TBST the next day and then incubated in secondary antibody solution (1:5000; Earthox) for 1 h at room temperature. The bands' signals were recorded by Quantity One software (Bio-Rad) using a Pierce ECL substrate kit (Millipore). β-Actin was used as the loading control.

Histopathological and immunohistochemical analyses

Mice were deeply anesthetized with pentobarbital, and the anterior abdominal wall was isolated followed by fixing in 4% paraformaldehyde. Then the tissues were dehydrated and embedded in paraffin. Before being stained, the paraffin was sliced and deparaffinized. The Masson's trichrome stain kit (G1006, Wuhan Servicebio Technology Co., Ltd., Wuhan, China) was used as the staining reagent. The thickness of the peritoneum was measured by randomly selecting five fields in each stained slice using a micrometer under the microscope. The means ± S.D. were used to analyze peritoneum thickness. Immunohistologically, paraffin sections (6 μm thick) were deparaffinized in xylene and rehydrated in alcohol with decreasing concentrations. Then the sections were immersed in sodium citrate antigen retrieval solution (pH 6.0) and maintained at a sub-boiling temperature for 8 min by a microwave oven (P70D20TL-P4, Glanze) to repair the antigen. After that, 3% H_2O_2 was used to block the endogenous peroxidase of samples at room temperature for 15 min in a dark place. Sections were then blocked with PBS containing 3% BSA for 30 min at 37 °C. After incubation with primary antibodies overnight at 4 °C, the samples were incubated with secondary antibody (GB23303, Servicebio) and counterstained with hematoxylin. The primary antibodies used in this study were anti-Col1α1 (1:500; ab34710, Abcam, Cambridge, MA) and anti-FGF10 (R&D Systems).

Immunofluorescence

For immunofluorescence, HMrSV5 cells were cultured on the glass coverslips in 6-well plates. When covering the bottom area of the 6-well plate by 60–70%, the cells were fixed in 4% paraformaldehyde solution. About 30 min later, cells were washed in PBS and then permeabilized with 0.3% Triton for 15 min. After that, the coverslips were blocked in 3% BSA in PBS-Tween (PBST) for 30 min at room temperature and then incubated with primary antibody at 4 °C overnight. The antibody used in this experiment was rabbit anti-ZEB1 (1:500; GB11513, Servicebio). The immunofluorescence of E-cad was performed when cells were confluently covering the bottom area of the 6-well plate. Mouse anti-E-cad (1:50; BD Biosciences) was used in the experiment. The coverslips were washed in PBST the next day, followed by Cy3-conjugated goat anti-rabbit IgG (1:300; GB21303, Servicebio) or FITC-conjugated goat anti-mouse IgG (1:300; GB22301, Servicebio) incubation for 50 min at room temperature. Finally, the nuclei were counterstained with 4′6′-diamino-2-phenylindole dihydrochloride (G1012, Servicebio). The fluorescence of ZEB1 was viewed with a Nikon Eclipse C1 upright fluorescence microscope (Nikon, Tokyo, Japan) and acquired using Nikon DS-U3 software. The E-cad fluorescence imaging was performed with the use of confocal laser-scanning microscopy (Leica SP8).

Luciferase reporter assay

To construct the luciferase reporter vectors, the nucleotide sequence of the FGF10 3′-UTR region containing the miR-145–binding sites was searched from a human cDNA library. The sequence is shown as Sequence S1. This region, which consists of 1451 bp, was amplified by RT-PCR. The sequence of 3′-UTR–specific primer was as follows: F-WT, 5′-AAA*GTTTAAAC*AGGAAGGCAACGTTTGTGG-3′ (with PmeI restriction site); R-WT 5′- AAA*GCGGCCGC*GGCTTATGTATTTATTTAGTGGAATAC-3′ (with NotI restriction site). The mutational constructs of FGF10 3′-UTR were obtained by replacing 5 nucleotides in the miR-145–binding site. Steps are as follows. First, primers containing mutated nucleotide sequences were designed. The sequence of F-mut was 5′-CGTAATACATGCAAGCATTT*TGACCT*AAGCAC-3′, and the sequence of R-mut was 5′-ATGATATGACCCAAGTGCTT*AGGTCA*AAATGC-3′. We used F-WT and R-mut primer to amplify a nucleotide sequence called fragment 1 and then used F-mut and R-WT to obtain fragment 2. The final mutated 3′-UTR of FGF10 was ligated from fragment 1 and fragment 2. The WT and mut nucleotide sequences of 3′-UTR were cloned into the psi-CHECK™-2 vector (Promega, Madison, WI) between the PmeI and NotI restriction sites (Fig. S4*D*). After plating HMrSV5 cells in 24-well plates, the two kinds of vectors were each cotransfected with ctrl mimics (25 pM) or miR-145 mimics (25 pM) using Lipofectamine 2000 reagent (11668019, Invitrogen). The luciferase activity was analyzed using luciferase assay kits (E1910, Promega) 24 h later. *Renilla* luciferase activity was normalized to that of firefly luciferase on a luminometer.

Statistical analysis

All data are expressed as the mean ± S.D. from at least three independent experiments. Statistical analysis was performed using one-way analysis of variance, followed by a two-tailed Student's *t* test with SPSS software. $p < 0.05$ was considered to indicate a statistically significant difference.

Author contributions—J. W., X. L., Z. X., Y. C., F. P., and H. L. conceptualization; J. W., Q. H., C. Z., W. G., C. L., and F. P. data curation; J. W., Q. H., B. Y., C. L., and W. Z. software; J. W., P. L., and X. L. validation; J. W., Q. H., P. L., Y. W., W. G., Y. C., and F. P. investigation; J. W. and S. L. visualization; J. W., Q. H., P. L., Y. W., B. Y., F. P., and H. L. methodology; J. W. writing-original draft; J. W. project administration; J. W. and H. L. writing-review and editing; P. L., J. X., F. P., and H. L. supervision; Y. W. and S. L. formal analysis; Y. C., F. P., and H. L. resources; H. L. funding acquisition.

Acknowledgments—We thank Prof. Jinjin Fan (Sun Yat-sen University) for providing the ultrasound transducer, Prof. Xueqing Yu (Sun Yat-sen University) for providing the HMrSV5 cells, and Longping Yao for kindly helping us analyze the experimental data.

References

1. Williams, J. D., Craig, K. J., Topley, N., Von Ruhland, C., Fallon, M., Newman, G. R., Mackenzie, R. K., Williams, G. T., and Peritoneal Biopsy Study Group (2002) Morphologic changes in the peritoneal membrane of patients with renal disease. *J. Am. Soc. Nephrol.* **13,** 470–479 Medline
2. Dhanakijcharoen, P., Sirivongs, D., Aruyapitipan, S., Chuengsaman, P., and Lumpaopong, A. (2011) The "PD First" policy in Thailand: three-years experiences (2008–2011). *J. Med. Assoc. Thai.* **94,** Suppl. 4, S153–S161 Medline
3. Rivara, M. B., and Mehrotra, R. (2014) The changing landscape of home dialysis in the United States. *Curr. Opin. Nephrol. Hypertens.* **23,** 586–591 CrossRef Medline
4. Stein, J. A. (2003) Peritoneal dialysis and epithelial-to-mesenchymal transition. *N. Engl. J. Med.* **348,** 2037–2039; author reply 2037–2039 CrossRef Medline
5. Patel, P., Sekiguchi, Y., Oh, K. H., Patterson, S. E., Kolb, M. R., and Margetts, P. J. (2010) Smad3-dependent and -independent pathways are involved in peritoneal membrane injury. *Kidney Int.* **77,** 319–328 CrossRef Medline
6. Margetts, P. J., and Bonniaud, P. (2003) Basic mechanisms and clinical implications of peritoneal fibrosis. *Perit. Dial. Int.* **23,** 530–541 Medline
7. López-Cabrera, M. (2014) Mesenchymal conversion of mesothelial cells is a key event in the pathophysiology of the peritoneum during peritoneal dialysis. *Adv. Med.* **2014,** 473134 Medline
8. Mutsaers, S. E., Birnie, K., Lansley, S., Herrick, S. E., Lim, C. B., and Prêle, C. M. (2015) Mesothelial cells in tissue repair and fibrosis. *Front. Pharmacol.* **6,** 113 Medline
9. Del Peso, G., Jimenez-Heffernan, J. A., Bajo, M. A., Aroeira, L. S., Aguilera, A., Fernandez-Perpen, A., Cirugeda, A., Castro, M. J., de Gracia, R., Sanchez-Villanueva, R., Sanchez-Tomero, J. A., Lopez-Cabrera, M., and Selgas, R. (2008) Epithelial-to-mesenchymal transition of mesothelial cells is an early event during peritoneal dialysis and is associated with high peritoneal transport. *Kidney Int. Suppl.* S26–S33 CrossRef Medline
10. Yao, L., Ye, Y., Mao, H., Lu, F., He, X., Lu, G., and Zhang, S. (2018) MicroRNA-124 regulates the expression of MEKK3 in the inflammatory pathogenesis of Parkinson's disease. *J. Neuroinflammation* **15,** 13 CrossRef Medline
11. Shang, J., He, Q., Chen, Y., Yu, D., Sun, L., Cheng, G., Liu, D., Xiao, J., and Zhao, Z. (2019) miR-15a-5p suppresses inflammation and fibrosis of peritoneal mesothelial cells induced by peritoneal dialysis via targeting VEGFA. *J. Cell. Physiol.* **234,** 9746–9755 CrossRef Medline
12. Che, M., Shi, T., Feng, S., Li, H., Zhang, X., Feng, N., Lou, W., Dou, J., Tang, G., Huang, C., Xu, G., Qian, Q., Sun, S., He, L., and Wang, H. (2017) The microRNA-199a/214 cluster targets E-cadherin and claudin-2 and promotes high glucose-induced peritoneal fibrosis. *J. Am. Soc. Nephrol.* **28,** 2459–2471 CrossRef Medline
13. Li, D., Lu, Z., Li, X., Xu, Z., Jiang, J., Zheng, Z., Jia, J., Lin, S., and Yan, T. (2018) Human umbilical cord mesenchymal stem cells facilitate the up-regulation of miR-153-3p, whereby attenuating MGO-induced peritoneal fibrosis in rats. *J. Cell. Mol. Med.* **22,** 3452–3463 CrossRef Medline
14. Ma, Y. L., Chen, F., Yang, S. X., Chen, B. P., and Shi, J. (2018) MicroRNA-21 promotes the progression of peritoneal fibrosis through the activation of the TGF-β/Smad signaling pathway: an *in vitro* and *in vivo* study. *Int. J. Mol. Med.* **41,** 1030–1038 Medline
15. Xiao, L., Zhou, X., Liu, F., Hu, C., Zhu, X., Luo, Y., Wang, M., Xu, X., Yang, S., Kanwar, Y. S., and Sun, L. (2015) MicroRNA-129-5p modulates epithelial-to-mesenchymal transition by targeting SIP1 and SOX4 during peritoneal dialysis. *Lab. Investig.* **95,** 817–832 CrossRef Medline
16. Zhou, Q., Yang, M., Lan, H., and Yu, X. (2013) miR-30a negatively regulates TGF-β1-induced epithelial-mesenchymal transition and peritoneal fibrosis by targeting Snai1. *Am. J. Pathol.* **183,** 808–819 CrossRef Medline
17. Liu, H., Zhang, N., and Tian, D. (2014) MiR-30b is involved in methylglyoxal-induced epithelial-mesenchymal transition of peritoneal mesothelial cells in rats. *Cell. Mol. Biol. Lett.* **19,** 315–329 CrossRef Medline
18. Yang, S., Cui, H., Xie, N., Icyuz, M., Banerjee, S., Antony, V. B., Abraham, E., Thannickal, V. J., and Liu, G. (2013) miR-145 regulates myofibroblast differentiation and lung fibrosis. *FASEB J.* **27,** 2382–2391 CrossRef Medline
19. Lutful Kabir, F., Ambalavanan, N., Liu, G., Li, P., Solomon, G. M., Lal, C. V., Mazur, M., Halloran, B., Szul, T., and Gerthoffer, W. T., Rowe, S. M., and Harris, W. T. (2018) MicroRNA-145 antagonism reverses TGF-β inhibition of F508del CFTR correction in airway epithelia. *Am. J. Respir. Crit. Care Med.* **197,** 632–643 CrossRef Medline
20. Men, R., Wen, M., Zhao, M., Dan, X., Yang, Z., Wu, W., Wang, M. H., Liu, X., and Yang, L. (2017) MircoRNA-145 promotes activation of hepatic stellate cells via targeting Kruppel-like factor 4. *Sci. Rep.* **7,** 40468 CrossRef Medline
21. Emoto, H., Tagashira, S., Mattei, M. G., Yamasaki, M., Hashimoto, G., Katsumata, T., Negoro, T., Nakatsuka, M., Birnbaum, D., Coulier, F., and Itoh, N. (1997) Structure and expression of human fibroblast growth factor-10. *J. Biol. Chem.* **72,** 23191–23194 CrossRef Medline
22. Watson, J., and Francavilla, C. (2018) Regulation of FGF10 signaling in development and disease. *Front. Genet.* **9,** 500 CrossRef Medline
23. Ornitz, D. M., and Itoh, N. (2015) The fibroblast growth factor signaling pathway. *Wiley Interdiscip. Rev. Dev. Biol.* **4,** 215–266 CrossRef Medline
24. Itoh, N. (2016) FGF10: a multifunctional mesenchymal-epithelial signaling growth factor in development, health, and disease. *Cytokine Growth Factor Rev.* **28,** 63–69 CrossRef Medline
25. Gupte, V. V., Ramasamy, S. K., Reddy, R., Lee, J., Weinreb, P. H., Violette, S. M., Guenther, A., Warburton, D., Driscoll, B., Minoo, P., and Bellusci, S. (2009) Overexpression of fibroblast growth factor-10 during both inflammatory and fibrotic phases attenuates bleomycin-induced pulmonary fibrosis in mice. *Am. J. Respir. Crit. Care Med.* **180,** 424–436 CrossRef Medline
26. Sun, W. L., Zhu, Y. P., Ni, X. S., Jing, D. D., Yao, Y. T., Ding, W., Liu, Z. H., Ding, G. X., and Jiang, J. T. (2018) Potential involvement of Fgf10/Fgfr2 and androgen receptor (AR) in renal fibrosis in adult male rat offspring subjected to prenatal exposure to di-*n*-butyl phthalate (DBP). *Toxicol. Lett.* **282,** 37–42 CrossRef Medline
27. Peinado, H., Olmeda, D., and Cano, A. (2007) Snail, Zeb and bHLH factors in tumour progression: an alliance against the epithelial phenotype? *Nat. Rev. Cancer* **7,** 415–428 CrossRef Medline
28. Skrypek, N., Bruneel, K., Vandewalle, C., De Smedt, E., Soen, B., Loret, N., Taminau, J., Goossens, S., Vandamme, N., and Berx, G. (2018) ZEB2 stably represses RAB25 expression through epigenetic regulation by SIRT1 and DNMTs during epithelial-to-mesenchymal transition. *Epigenetics Chromatin* **11,** 70 CrossRef Medline
29. Correll, K. A., Edeen, K. E., Redente, E. F., Zemans, R. L., Edelman, B. L., Danhorn, T., Curran-Everett, D., Mikels-Vigdal, A., and Mason, R. J.

(2018) TGF β inhibits HGF, FGF7, and FGF10 expression in normal and IPF lung fibroblasts. *Physiol. Rep.* **6,** e13794 CrossRef Medline

30. Bartel, D. P. (2009) MicroRNAs: target recognition and regulatory functions. *Cell* **136,** 215–233 CrossRef Medline
31. Shirakihara, T., Horiguchi, K., Miyazawa, K., Ehata, S., Shibata, T., Morita, I., Miyazono, K., and Saitoh, M. (2011) TGF-β regulates isoform switching of FGF receptors and epithelial-mesenchymal transition. *EMBO J.* **30,** 783–795 CrossRef Medline
32. Zeisberg, M., and Neilson, E. G. (2009) Biomarkers for epithelial-mesenchymal transitions. *J. Clin. Invest.* **119,** 1429–1437 CrossRef Medline
33. Nieto, M. A., Huang, R. Y., Jackson, R. A., and Thiery, J. P. (2016) EMT: 2016. *Cell* **166,** 21–45 CrossRef Medline
34. Kalluri, R., and Weinberg, R. A. (2009) The basics of epithelial-mesenchymal transition. *J. Clin. Invest.* **119,** 1420–1428 CrossRef Medline
35. Tulchinsky, E., Demidov, O., Kriajevska, M., Barlev, N. A., and Imyanitov, E. (2019) EMT: a mechanism for escape from EGFR-targeted therapy in lung cancer. *Biochim. Biophys. Acta Rev. Cancer* **1871,** 29–39 CrossRef Medline
36. Yáñez-Mó, M., Lara-Pezzi, E., Selgas, R., Ramírez-Huesca, M., Domínguez-Jimenez, C., Jiménez-Heffernan, J. A., Aguilera, A., Sánchez-Tomero, J. A., Bajo, M. A., Alvarez, V., Castro, M. A., del Peso, G., Cirujeda, A., Gamallo, C., Sánchez-Madrid, F., and López-Cabrera, M. (2003) Peritoneal dialysis and epithelial-to-mesenchymal transition of mesothelial cells. *N. Engl. J. Med.* **348,** 403–413 CrossRef Medline
37. Liu, Y., Dong, Z., Liu, H., Zhu, J., Liu, F., and Chen, G. (2015) Transition of mesothelial cell to fibroblast in peritoneal dialysis: EMT, stem cell or bystander? *Perit. Dial. Int.* **35,** 14–25 CrossRef Medline
38. Shin, H. S., Ryu, E. S., Oh, E. S., and Kang, D. H. (2015) Endoplasmic reticulum stress as a novel target to ameliorate epithelial-to-mesenchymal transition and apoptosis of human peritoneal mesothelial cells. *Lab. Invest.* **95,** 1157–1173 CrossRef Medline
39. Selgas, R., Bajo, A., Jiménez-Heffernan, J. A., Sánchez-Tomero, J. A., Del Peso, G., Aguilera, A., and López-Cabrera, M. (2006) Epithelial-to-mesenchymal transition of the mesothelial cell—its role in the response of the peritoneum to dialysis. *Nephrol. Dial. Transplant.* **21,** Suppl. 2, ii2–ii7 CrossRef Medline
40. Strippoli, R., Loureiro, J., Moreno, V., Benedicto, I., Pérez Lozano, M. L., Barreiro, O., Pellinen, T., Minguet, S., Foronda, M., Osteso, M. T., Calvo, E., Vázquez, J., López Cabrera, M., and del Pozo, M. A. (2015) Caveolin-1 deficiency induces a MEK-ERK1/2-Snail-1-dependent epithelial-mesenchymal transition and fibrosis during peritoneal dialysis. *EMBO Mol. Med.* **7,** 102–123 CrossRef Medline
41. Vargha, R., Bender, T. O., Riesenhuber, A., Endemann, M., Kratochwill, K., and Aufricht, C. (2008) Effects of epithelial-to-mesenchymal transition on acute stress response in human peritoneal mesothelial cells. *Nephrol. Dial. Transplant.* **23,** 3494–3500 CrossRef Medline
42. Yu, J. W., Duan, W. J., Huang, X. R., Meng, X. M., Yu, X. Q., and Lan, H. Y. (2014) MicroRNA-29b inhibits peritoneal fibrosis in a mouse model of peritoneal dialysis. *Lab. Invest.* **94,** 978–990 CrossRef Medline
43. Kokoroishi, K., Nakashima, A., Doi, S., Ueno, T., Doi, T., Yokoyama, Y., Honda, K., Kanawa, M., Kato, Y., Kohno, N., and Masaki, T. (2016) High glucose promotes TGF-β1 production by inducing FOS expression in human peritoneal mesothelial cells. *Clin. Exp. Nephrol.* **20,** 30–38 CrossRef Medline
44. Wang, L., Liu, N., Xiong, C., Xu, L., Shi, Y., Qiu, A., Zang, X., Mao, H., and Zhuang, S. (2016) Inhibition of EGF receptor blocks the development and progression of peritoneal fibrosis. *J. Am. Soc. Nephrol.* **27,** 2631–2644 CrossRef Medline
45. Zhao, S., Jiang, J. T., Li, D., Zhu, Y. P., Xia, S. J., and Han, B. M. (2019) Maternal exposure to di-*n*-butyl phthalate promotes Snail1-mediated epithelial-mesenchymal transition of renal tubular epithelial cells via up-regulation of TGF-β1 during renal fibrosis in rat offspring. *Ecotoxicol. Environ. Safety* **169,** 266–272 CrossRef Medline
46. Shin, H. S., Ko, J., Kim, D. A., Ryu, E. S., Ryu, H. M., Park, S. H., Kim, Y. L., Oh, E. S., and Kang, D. H. (2017) Metformin ameliorates the phenotype transition of peritoneal mesothelial cells and peritoneal fibrosis via a modulation of oxidative stress. *Sci. Rep.* **7,** 5690 CrossRef Medline
47. Chang, H. Y., Chi, J. T., Dudoit, S., Bondre, C., van de Rijn, M., Botstein, D., and Brown, P. O. (2002) Diversity, topographic differentiation, and positional memory in human fibroblasts. *Proc. Natl. Acad. Sci. U.S.A.* **99,** 12877–12882 CrossRef Medline
48. Zhou, D. D., Wang, X., Wang, Y., Xiang, X. J., Liang, Z. C., Zhou, Y., Xu, A., Bi, C. H., and Zhang, L. (2016) MicroRNA-145 inhibits hepatic stellate cell activation and proliferation by targeting ZEB2 through Wnt/β-catenin pathway. *Mol. Immunol.* **75,** 151–160 CrossRef Medline
49. Rougier, J. P., Moullier, P., Piedagnel, R., and Ronco, P. M. (1997) Hyperosmolality suppresses but TGF β 1 increases MMP9 in human peritoneal mesothelial cells. *Kidney Int.* **51,** 337–347 CrossRef Medline